Chemistry–A European Journal
Research Article
doi.org/10.1002/chem.202300075
Chemistry Europe
European Chemical Societies Publishing
www.chemeurj.org

Detection of Large Genomic RNA via DNAzyme-Mediated RNA Cleavage and Rolling Circle Amplification: SARS-CoV-2 as a Model

Jimmy Gu[+],[a, b] Amal Mathai[+],[a, b] Connor Nurmi[+],[a, b] Dawn White,[c] Gurpreet Panesar,[a] Deborah Yamamura,[b, e] Cynthia Balion,[e] Jonathan Gubbay,[i] Karen Mossman,[d] Alfredo Capretta,[b, c] Bruno J. Salena,[d] Leyla Soleymani,[f, g] Carlos D. M. Filipe,[h] John D. Brennan,*[c] and Yingfu Li*[a, b, c, g]

Abstract: A new method for the detection of genomic RNA combines RNA cleavage by the 10-23 DNAzyme and use of the cleavage fragments as primers to initiate rolling circle amplification (RCA). 230 different 10-23 DNAzyme variants were screened to identify those that target accessible RNA sites within the highly structured RNA transcripts of SARS-CoV-2. A total of 28 DNAzymes were identified with >20% cleavage, 5 with >40% cleavage and one with >60% in 10 min. The cleavage fragments from these reactions were then screened for coupling to an RCA reaction, leading to the identification of several cleavage fragments that could efficiently initiate RCA. Using a newly developed quasi-exponential RCA method with a detection limit of 500 aM of RNA, 14 RT-PCR positive and 15 RT-PCR negative patient saliva samples were evaluated for SARS-CoV-2 genomic RNA, achieving a clinical sensitivity of 86% and specificity of 100% for detection of the virus in <2.5 h.

Introduction

Effective detection of cancer and bacterial or viral pathogens is critical for ensuring positive health outcomes at the individual and community level. Many diagnostic methods have been successfully developed that utilize genomic ribonucleic acid (RNA) as a target biomolecule for a diverse range of applications including detection of breast and prostate cancers,[1–6] bacterial contamination in municipal drinking waters[7] and viral infections including SARS-CoV-2.[8–11] Nucleic acid amplification tests (NAATs) for detection of clinically relevant RNA often combine reverse transcription (RT) with an amplification step such as polymerase chain reaction (RT-PCR) to achieve ultra-sensitive detection.[12–15]

Isothermal NAATs, including those employing loop-mediated isothermal amplification (LAMP) and recombinase polymerase amplification (RPA), also provide high sensitivity and selectivity for clinical diagnosis and avoid the need for a thermocycler.[16,17]

[a] J. Gu,[+] A. Mathai,[+] C. Nurmi,[+] G. Panesar, Prof. Dr. Y. Li
Department of Biochemistry and Biomedical Sciences
McMaster University
1280 Main Street West, Hamilton, Ontario, L8S 4K1 (Canada)
E-mail: liying@mcmaster.ca

[b] J. Gu,[+] A. Mathai,[+] C. Nurmi,[+] Prof. Dr. D. Yamamura, Prof. Dr. A. Capretta, Prof. Dr. Y. Li
Michael G. DeGroote Institute of Infectious Disease Research
McMaster University
1280 Main Street West, Hamilton, Ontario, L8S 4K1 (Canada)

[c] D. White, Prof. Dr. A. Capretta, Prof. Dr. J. D. Brennan, Prof. Dr. Y. Li
Biointerfaces Institute
McMaster University
1280 Main Street West, Hamilton, Ontario, L8S 4K1 (Canada)
E-mail: brennanj@mcmaster.ca

[d] Prof. Dr. K. Mossman, Prof. Dr. B. J. Salena
Department of Medicine
McMaster University
1280 Main Street West, Hamilton, Ontario, L8S 4K1 (Canada)

[e] Prof. Dr. D. Yamamura, Prof. Dr. C. Balion
Department of Pathology and Molecular Medicine
McMaster University
1280 Main Street West, Hamilton, Ontario, L8S 4K1 (Canada)

[f] Prof. Dr. L. Soleymani
Department of Engineering Physics
McMaster University
1280 Main Street West, Hamilton, Ontario, L8S 4K1 (Canada)

[g] Prof. Dr. L. Soleymani, Prof. Dr. Y. Li
School of Biomedical Engineering
McMaster University
1280 Main Street West, Hamilton, Ontario, L8S 4K1 (Canada)

[h] Prof. Dr. C. D. M. Filipe
Department of Chemical Engineering
McMaster University
1280 Main Street West, Hamilton, Ontario, L8S 4K1 (Canada)

[i] Dr. J. Gubbay
Public Health Ontario Laboratory
Toronto, Ontario (Canada)

[+] These authors contributed equally to this work.

Supporting information for this article is available on the WWW under https://doi.org/10.1002/chem.202300075

Although highly sensitive, these amplification methods typically require specialized equipment, experience long processing times and must be performed by laboratory technicians. Additionally, RT-based RNA detection methods commonly suffer from false-positive results as cross-hybridization of nucleic acid targets with similar sequences can occur.[18] These methods also often require expensive reagents that are temperature-sensitive, require complex primer and probe design and multiple reaction steps. Thus, improved diagnostic methods to directly detect large genomic RNA targets are needed. These methods should feature specific molecular recognition of target RNA sequences and couple with a highly sensitive amplification method that can be performed under isothermal conditions to produce a rapid and robust result.

Rolling circle amplification (RCA) is a nucleic acid amplification reaction that uses a highly processive phi29 DNA polymerase (ϕ29DP) that extends the 3′-end of a linear nucleic acid primer around a circular DNA template (CDT). The resulting long, concatenated reaction products (RPs) can be detected with high sensitivity using many methods, including fluorometrically (using fluorophore-conjugated probes or intercalating dyes) or colorimetrically (using gold nanoparticle hybridization).[19–22] RCA assays have been widely used for detection of short RNA sequences, such as microRNA targets, as these can directly bind to complementary CDTs to initiate amplification and generate sensitive output signals.[23–25] However, direct detection of large genomic RNA by RCA has yet to be demonstrated. Given that some viral genomes, such as that of SARS-CoV-2, contain over 30,000 nucleotides[26] but only a single 3′-end, hybridization of the 3′-end to the CDT becomes challenging, as the termini may be sequestered within higher-order structural elements or digested by nucleases in biological samples, producing undefined 3′-ends.

In this study we have developed a novel, large RNA detection method based on the use of RNA-cleaving DNAzymes (RCDs) to produce well defined primers from genomic RNA that can bind to a CDT to prime RCA. We hypothesized that a properly designed RCD should be able to bind to a genomic RNA sequence at a desired internal site and selectively cleave the RNA to produce a 3′-terminal segment that can bind a CDT to prime RCA. Figure 1 outlines the overall design of the strategy using the genome of SARS-CoV-2 as an example. The RCD selectively cuts the viral RNA of SARS-CoV-2 at a specific target site to generate two RNA fragments, where the 3′-end of the 5′ cleavage fragment (Step **I** in Figure 1) binds to a CDT (Step **II**), followed by ϕ29DP-catalyzed RCA to produce a reaction product (Step **III**), which can either be fed back into an exponential RCA reaction to achieve improved detection limits, or be detected directly using a DNA-binding fluorogenic dye (Step **IV**).

For assay development, we investigated the 10-23 DNAzyme, initially reported by Santoro and Joyce,[27] for cleavage of genomic RNA transcripts from SARS-CoV-2, as it possesses high RNA cleavage activity under diverse reaction conditions. The 10-23 DNAzyme contains a relatively simple catalytic core consisting of 15 conserved DNA nucleotides, and cleaves purine and pyrimidine junctions with the greatest activity observed for

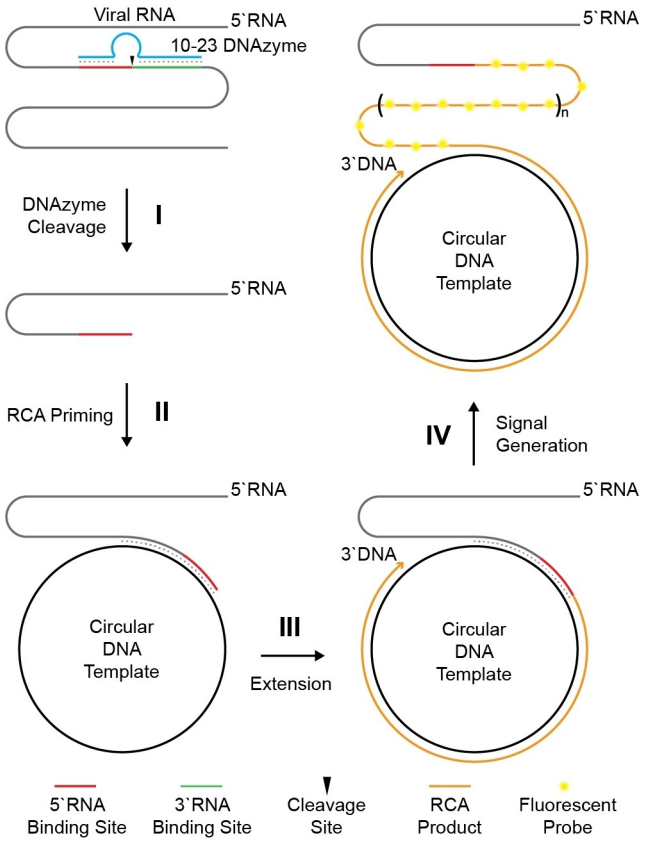

Figure 1. Overview of DNAzyme directed primer generation coupled to RCA for detection of SARS-CoV-2 genomic RNA. Viral genomic RNA is site specifically cleaved by a 10-23 DNAzyme. The newly generated 3′ RNA terminal serves as a primer for RCA.

A–U or G–U dinucleotide junctions.[28] Importantly, the binding arms of the 10-23 DNAzyme can be varied, as their length and sequence composition do not have a significant effect on the rate of RNA cleavage. Thus, the sequence of the binding arms of this DNAzyme can be modified to target different A–U or G–U junctions along the length of a genomic RNA sequence, producing highly predictable cleavage products that can act as primers to initiate RCA.

Given that naturally occurring RNA molecules tend to form strong secondary structures due to a multitude of intramolecular base-pairing interactions,[29–31] we utilized a combination of secondary structure prediction and experimentation to screen 230, 10-23 DNAzymes possessing different binding arms to identify RCDs that could bind and cleave at specific sites within the SARS-CoV-2 genome. We show that this screening method can rapidly identify multiple 10-23 DNAzymes with relatively high cleavage activity that can be further screened for their effectiveness in coupling with CDTs to prime RCA. Using a newly developed quasi-exponential RCA method, we demonstrate that the combined DNAzyme-RCA assay can achieve sub-femtomolar detection of RNA at room temperature without the need of an RT step. We have successfully applied this assay for detection of SARS-CoV-2 genomic RNA in minimally processed

patient saliva samples, showing excellent agreement with traditional RT-PCR assays.

Results and Discussion

Designing 10-23 DNAzyme variants targeting SARS-CoV-2 RNA for cleavage

Naturally occurring RNA molecules are known to have substantial secondary structure, so not all potential cleavage sites for 10-23 DNAzymes are accessible. We hypothesized that we could use a combination of secondary structure prediction and cleavage activity screening to identify highly accessible sites within the ~30,000 nucleotide SARS-CoV-2 RNA genome (consisting of 13–15 open reading frames)[32] that allowed efficient 10-23 DNAzyme binding and cleavage to yield RNA primers to initiate RCA.

In this study, long RNA transcripts were used as substrates to reflect naturally occurring secondary structures. Although the RNA transcripts were indeed shorter than the full SARS-CoV-2 genomic RNA, localized secondary structures that could prevent 10-23 DNAzyme accessibility to the target site were expected to remain intact.[33] We prepared 20 RNA transcripts from PCR products encoding gene fragments of the original SARS-CoV-2 virus. The Membrane (M), Nucleocapsid (N), ORF3a, NSP1, NSP2, NSP3, NSP5, NSP6, NSP8, NSP13, NSP14, NSP15 and NSP16 genes were produced as single transcripts (see Table S1 in the Supporting Information); however, the NSP12 and Spike (S) transcripts were split into 2 and 5 shorter transcripts, respectively, to simplify transcription and electrophoretic analysis. Each RNA transcript was radiolabeled with ^{32}P at its 5′-end and gel-purified prior to 10-23 DNAzyme-mediated cleavage. RNA transcript sizes ranged from 478 to 1916 nucleotides (see Table S1), contained between 4 and 28 potential cleavage sites (Figure S1), and collectively covered ~70% of the entire SARS-CoV-2 genome.

RNA sites for 10-23 DNAzyme cleavage were selected based on two main criteria: 1) the presence of a G–U or A–U dinucleotide junction, for which the 10-23 DNAzyme is known to have the highest activity; and 2) the accessibility of the cleavage site based on a predicted RNA secondary structure.[34] Sequences of the RNA transcripts were folded using the ViennaRNA website's RNAfold server to generate a minimum free energy structure prediction and pairing probability structure.[35] Suitable dinucleotide junctions were mapped onto the pairing probability structure and target sites were manually selected based on the presence of high-probability unpaired regions adjacent to the RNA cleavage site. An effort was also made to select sites without strong pairing in the post-cleavage 5′-RNA fragment as these may inhibit binding of a CDT for priming the subsequent RCA reaction. In most cases, the selected cleavage sites were located in loop regions, bulges or junctions.

Figure 2A illustrates the predicted RNA secondary structure of the 1583 nt NSP14 transcript as an example of the 20 transcripts examined in this study. Based on the predicted secondary structure and the requirement that a G–U or A–U site is located within a single stranded region, adjacent to a single-stranded region or near a junction, we designed 19 variants of the 10-23 DNAzyme targeting NSP14 (see Table S2 for the sequences of all tested 10-23 DNAzyme variants), of which the 16 longest 5′-fragments are indicated in Figure 2A. Figure 2B provides the sequence and local secondary structure of the RNA site labelled ⑪, which is targeted by a 10-23 DNAzyme named "dZ 18973a". The naming convention of screened DNAzymes includes the "dZ" prefix for 10-23 DNAzyme followed by the nucleotide position of the 5′ nucleotide in the targeted dinucleotide cleavage junction referenced to the SARS-CoV-2 reference sequence (GenBank record MN908947.3).[32] A lowercase letter suffix indicates a binding arm configuration corresponding to 8 pairing nucleotides upstream and 15 pairing nucleotides downstream of the targeted dinucleotide junction with the 5′ nucleotide of the junction remaining unpaired. In the case of dZ 18973a, the cleavage site is G–U (indicated in red) and the upstream and downstream RNA sequences that the two binding arms of the DNAzyme complement are shown in green. The predicted formation of the DNAzyme/RNA complex is represented in Figure 2C (note that the sequence of dZ 18973a is shown in blue). With the formation of this DNAzyme/RNA substrate complex, dZ 18973a is positioned to cleave the RNA between G936 and U937, breaking the 1583 nt NSP14 RNA transcript into two fragments, radioactive 936 nt 5′-fragment P1 and non-radioactive 647 nt 3′-fragment P2. Both the initial transcript and P1 could be detected via denaturing polyacrylamide gel electrophoresis (dPAGE) followed by phosphorimaging (Figure 2D) while nonradioactive P2 was undetectable by this technique.

RNA cleavage reactions were performed under single-turnover conditions ([DNAzyme] = 500 nM and [transcript] = 50 nM) in a reaction buffer containing 50 mM HEPES (pH 7.4), 10 mM $MgCl_2$, 100 mM NaCl. The reaction buffer contained higher levels of Mg^{2+} compared to physiological Mg^{2+} levels (1–2 mM) to maximize 10-23 DNAzyme activity (see Figure S2). The cleavage reaction was conducted at 23 °C for 10 min, and the reaction mixture was analyzed by 5% dPAGE to calculate the percent cleavage (Y_{10}), which is defined as $Y_{10} = [R_{P1}/(R_{RNA} + R_{P1})]$ x 100, where R_{RNA} and R_{P1} represent the integrated density of the uncleaved RNA transcript band and the P1 cleavage product band on a storage phosphor image, respectively. The Y_{10} values were determined for the 16 DNAzymes designed for NSP14 RNA and are provided at the bottom of Figure 2D. Among these DNAzymes, 11 exhibited clearly detectable activity in the 10-min reaction time (Figure 2D). However, the Y_{10} values of these DNAzymes varied significantly, from 2%–34%. For this set of 16 DNAzymes, dZ 18583a was found to be the most active, achieving a Y_{10} value of 34% over 10 min.

Screening a large set of 10-23 DNAzymes to search for variants with potent cleavage activities

Using the method described above for the NSP14 transcript, we designed 10-23 DNAzymes targeting 230 sequence elements

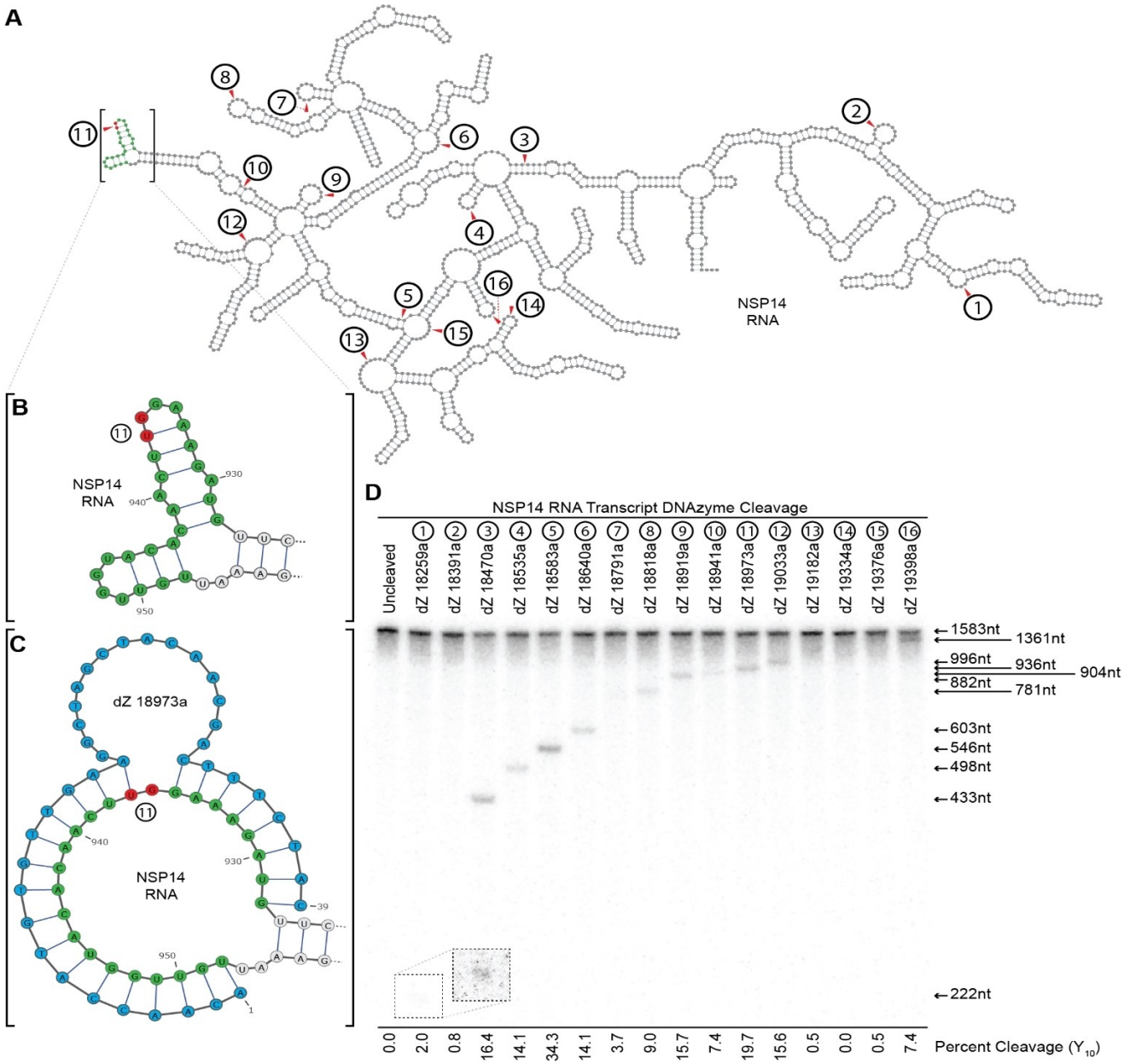

Figure 2. Representative predicted RNA secondary structure, DNAzyme binding site and cleavage site screening reactions. (A) Secondary structure of SARS-CoV-2 RNA transcript encoding NSP14 as predicted using RNAfold. (B) Sequence and local predicted structure of RNA site targeted by dZ 18973a (DNAzyme binding region in green; cleavage junction dinucleotides in red). (C) Sequences and structure of predicted complex between the RNA substrate and dZ 18973a DNAzyme in blue. The 10-23 catalytic core is positioned to cleave the RNA between 936G-937U (red). (D) Denaturing PAGE analysis of 5′-^{32}P labelled SARS-CoV-2 NSP14 RNA transcripts after cleavage by candidate DNAzymes.

across 20 transcripts (see Table S1 and Figure S1 for the distribution of the DNAzymes using these transcripts). The Y_{10} values were determined for all 230 DNAzymes and the data are organized into Figure 3 (see Figures S3–S17 for RNA folds and target sites of DNAzymes with $Y_{10} \geq 20\%$). Careful analysis of Figure 3 reveals several interesting findings.

First, many DNAzymes show robust activities. Specifically, 28 DNAzymes (12.2% of all DNAzyme constructs) produced a Y_{10} value of $\geq 20\%$, 5 DNAzymes (2.2%) exhibited a Y_{10} value of $\geq 40\%$, and one DNAzyme (0.4%) had a Y_{10} above 60% (dZ 13726a targeting NSP12 for cleavage and exhibiting a Y_{10} value of 64%). These observations support the effectiveness of designing and testing hundreds of 10–23 DNAzyme variants targeting transcripts of a relatively large RNA genome such as that of SARS-CoV-2, as it can generate a pool of highly active DNAzymes in a timely and cost-effective fashion. (The entire experiment can be completed in a week; each DNAzyme costs less than $10 to produce.)

Second, the number of DNAzymes designed for each of the 15 genes varies between 4 (M gene) and 28 (NSP3), with 15 sites targeted on average (Figure S1). However, screening of a larger number of DNAzymes does not always translate to the

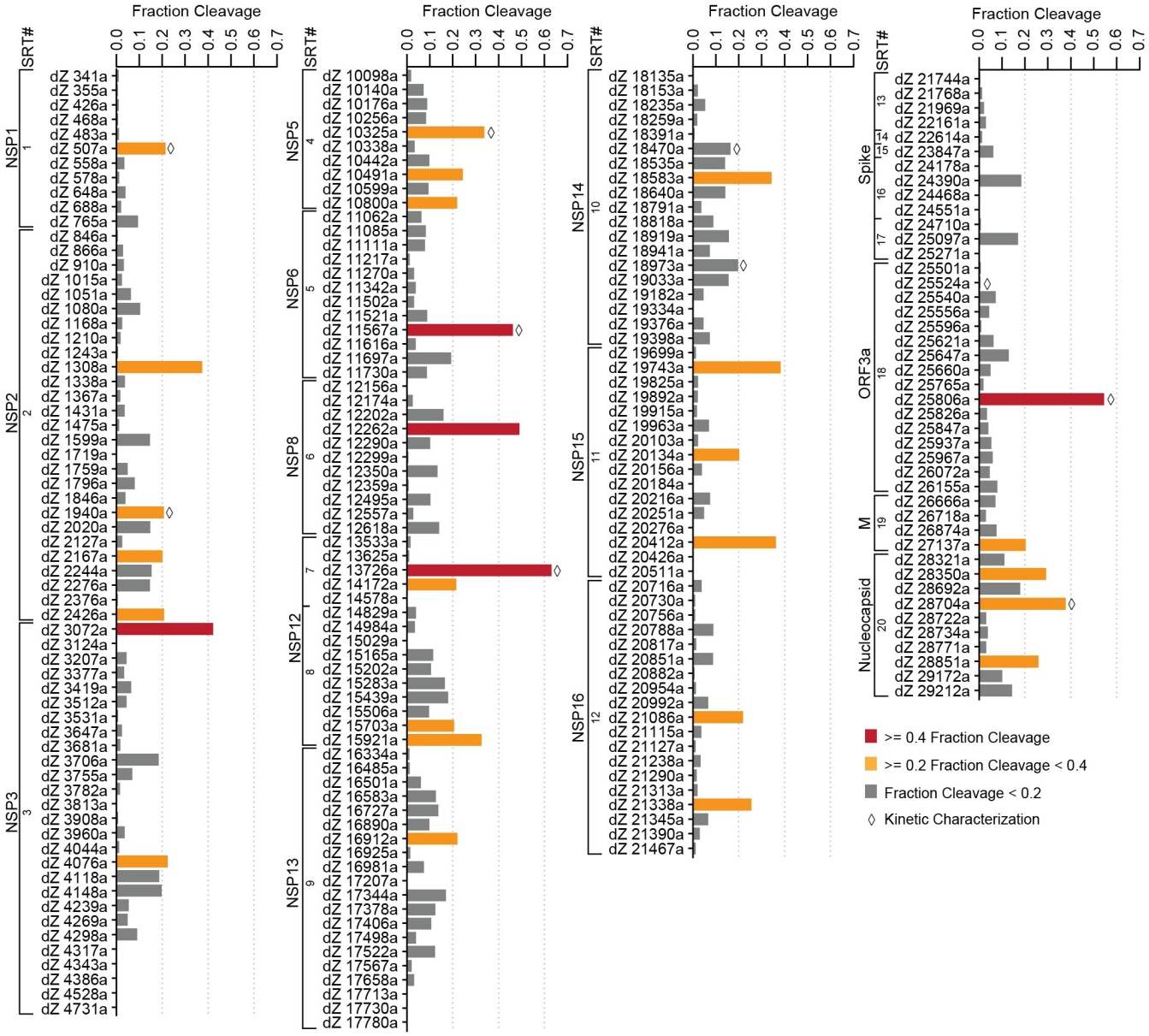

Figure 3. Summary of DNAzyme cleavage activity at target sites across 15 regions of the SARS-CoV-2 genome. Single turnover reactions were performed using DNAzyme and 5′-^{32}P labelled RNA transcripts. Bars represent percent cleavage at 10 min (Y_{10}) and 23 °C under single-turnover conditions.

identification of a greater number of effective DNAzymes. For example, 28 DNAzymes were designed and tested for NSP3, which only produced two DNAzymes with $Y_{10} \geq 20\,\%$; in contrast, only 4 DNAzymes were screened for the M gene, which nevertheless produced one DNAzyme with $Y_{10} \geq 20\,\%$.

Third, in several instances, dramatic differences in Y_{10} values are observed between DNAzymes with adjacent cleavage sites. For example, dZ 25806a and dZ 25826a were designed to target two cleavage sites within ORF3a that are only 20 nt apart; dZ 25806a is highly active ($Y_{10} = 54\,\%$), but dZ 25826a has minimal activity ($Y_{10} = 2\,\%$). The dZ 20412a and dZ 20426a pair constitutes another example: the activity of dZ 20412a is quite high ($Y_{10} = 36\,\%$) while dZ 20426a is completely inactive ($Y_{10} = 0$) even though the two DNAzymes target cleavage sites separated by only 14 nucleotides.

To better understand these effects, we used DNAzyme cleavage activity from the screening study to perform a statistical analysis aimed at identifying correlations between cleavage activity and predicted free energies of folded DNAzyme and RNA target sequences (ΔG_{fold}). Statistically significant correlations were identified between log cleavage fraction and ΔG_{fold} parameters of 1) the DNAzyme sequence, 2) the RNA binding site, 3) a 25 nt RNA region flanking the DNAzyme binding site and 4) a 50 nt region flanking the DNAzyme binding site (Table S3). The greatest correlation (Pearson coefficient 0.343, p-value < 0.05) was observed with

the ΔG_{fold} of the folded DNAzyme sequence, indicating higher cleavage activity trends positively with weaker DNAzyme ΔG_{fold}.

Similarly, weaker correlations observed with the other parameters were consistent with higher cleavage activity trending with lower opening energies of DNAzyme binding sites, and lower ΔG_{fold} of RNA regions proximal to the DNAzyme binding site. However, low correlation coefficients in this analysis suggest additional factors remain unidentified in explaining the significant variations observed in cleavage activity across the screen. These factors may include types of secondary structure interactions not predicted by nucleic acid folding algorithms, tertiary interactions, or three-dimensional structural features.

Overall, the above observations clearly indicate that the secondary structures of DNAzymes as well as the secondary and tertiary structures of RNA targets are major factors in determining whether a given cleavage site is accessible to and can be cleaved by a DNAzyme.

A highly active DNAzyme must bind its substrate using the two binding arms and position its catalytic core optimally relative to the dinucleotide junction to be cleaved. This means that the DNAzyme must adopt the correct structure for binding, while the RNA cleavage site and its upstream and downstream sequences must be available for the DNAzyme to bind. However, the intrinsic secondary and tertiary structures of these species may be too strong for a DNAzyme to overcome as seen with most of the target sites (i.e., 87.8% of the tested sites with $Y_{10} < 20\%$). This clearly shows that while secondary structure prediction algorithms can inform cleavage site selection and DNAzyme binding arm design, experimental testing is necessary to probe if a desired site is actually targetable and whether the secondary structure of a given DNAzyme (that may arise from the binding arms) might prevent its binding to the targeted RNA sequence.

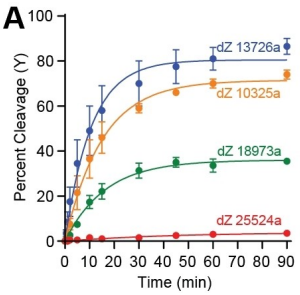

DNAzyme	Y_{10}(%)	Y_{10}'(%)	k_{obs}(min^{-1})	Y_{max}(%)
dZ 13726a	63.1	49.0	0.094	80.5
dZ 25806a	55.5	51.5	0.090	85.6
dZ 11567a	46.2	43.0	0.110	62.4
dZ 28704a	37.8	46.6	0.073	86.9
dZ 10325a	33.8	36.5	0.066	71.0
dZ 507a	21.4	22.1	0.030	87.0
dZ 1940a	20.7	29.0	0.065	53.8
dZ 18973a	19.7	17.4	0.062	36.0
dZ 18470a	16.4	16.0	0.037	51.8
dZ 12618a	14.0	16.0	0.029	62.5
dZ 25524a	0.6	1.5	0.022	4.0

Figure 4. (A) Kinetic characterization of select DNAzyme candidates. Representative cleavage reactions of four DNAzymes against their matching RNA substrates. Mean data points, SD and best-fit curve ($Y = Y_{max}(1-e^{-kt})$) are plotted. Y_{10} = percent cleavage from screen. Y_{10}' = percentage cleavage at 10 min kinetic assay. (B) Summarized screening cleavage fraction and observed rate constants for eleven DNAzymes selected for kinetic characterization.

Kinetic analysis of top 11 DNAzymes from the screening experiment

The DNAzyme/substrate activity screening experiments presented above were performed under conditions of single turnover ([DNAzyme]/[substrate] = 10) at a single timepoint (10 min) as a rapid way to identify the most active 10-23 DNAzyme variants among the large set of DNAzyme/substrate pairs (230 pairs in total). To confirm the screening results, 11 DNAzymes were chosen for more thorough kinetic analysis.

Duplicate dPAGE gels were run for each DNAzyme (representative gels for dZ 13726a are shown in Figure S18) and the kinetic profiles of four representative DNAzymes are provided in Figure 4A (those of the remaining seven can be found in Figure S19). DNAzymes across a range of Y_{10} values were selected for this analysis, including five DNAzymes with high activity ($Y_{10} > 30\%$), and six DNAzymes with low activity ($Y_{10} \leq 20\%$) (Column Y_{10}, Figure 4B). The data were then fitted using $Y = Y_{max}(1-e^{-kt})$ to derive the observed rate constant (Column k_{obs}, Figure 4B) and maximal percent cleavage (Column Y_{max}, Figure 4B) for the DNAzymes tested. To assess whether a second inactive conformation with a slow conversion rate might exist, we also fit a biphasic model for two DNAzymes with low activity, dZ 25524a and dZ 18973a, based on $Y = Y_{max1}(1-e^{-k1t}) + Y_{max2}(1-e^{k2t})$; however, the observed fits and rate constants did not improve (see Figure S20). We also re-determined Y_{10} values in this experiment and listed them in column Y_{10}' of Figure 4B.

Three outcomes from the above experiments are worth noting. First, the Y_{10} and Y_{10}' values for all DNAzymes are quite consistent, suggesting the single-point screening data presented in Figure 3 is reliable. Second, DNAzymes with $Y_{10} > 30\%$ (the first 5 DNAzymes listed in Figure 4B) exhibit higher k_{obs} values than those with $Y_{10} \leq 20\%$ (the last 6 DNAzymes), which is consistent with the ranking established with Y_{10} and Y_{10}' values. For example, the top three DNAzymes ranked by Y_{10} were also the same DNAzymes that produced the top three k_{obs} values. Third, the Y_{max} values vary significantly, from 4.0% (dZ 25524a) to 87.0% (dZ 507a). Once again, top DNAzymes by Y_{10} ranking exhibit generally better Y_{max} values than those with lower Y_{10} values. The exception is dZ 507a, which has a relatively low Y_{10} value (20%) but a high Y_{max} value (87.0%). The likely explanation for the poor Y_{max} values for some of the DNAzyme/substrate pairs is that the targeted RNA site in these pairs may exist as two conformational populations, one that is accessible to the DNAzyme and one that does not allow the DNAzyme to bind. Ideal DNAzyme candidates and corresponding target sites would possess high rate (k_{obs}) and high Y_{max} parameters to rapidly generate many cleavage products for coupling to RCA for amplified detection. Taken together, the above analysis suggests that screening a large set of DNAzymes can rapidly reveal excellent cleavage options targeting accessible regions of large genomic RNA like the SARS-CoV-2 RNA genome.

To further evaluate the impact of secondary or tertiary structure of the RNA substrate on DNAzyme rate constants, kinetic analyses were done on five DNAzymes using both the original long RNA transcript and a shorter RNA substrate of only 25 nt, matching the length of the binding arms. All five DNAzymes tested exhibited an increase in catalytic rate with the 25 nt RNA substrate compared to the larger RNA substrate

(Table S4). This was particularly evident with transcripts that had low cleavage rates, with the least active DNAzyme from the screen, dZ 25524a, showing nearly a 200-fold improvement in activity for the 25 nt sequence when compared to the rate with the 831 nt RNA substrate. These data show that DNAzyme cleavage activity of the full RNA transcript was significantly reduced relative to short RNA transcripts owing to the binding and/or cleavage sites being less accessible to the DNAzyme.

Coupling DNAzyme cleavage fragments to RCA

We next examined the coupling of the DNAzyme mediated RNA cleavage reactions to RCA. Once again, we took a screening approach to quickly assess 34 DNAzyme/substrate pairs to obtain systems capable of performing both efficient RNA cleavage and RCA (see Figure S21 for the sequences of CDTs and the RNA cleavage fragments used as the RCA primer for each of the 34 pairs). Our goal was to develop a saliva-based diagnostic test, and thus we performed coupled DNAzyme-RCA reactions in the presence of 50% human saliva. Several saliva sample treatment procedures were compared to identify a condition where RNA was protected from salivary nucleases (Figure S22). Based on this data, the following optimized method was used.

Prior to coupled DNAzyme-RCA reactions, saliva samples were treated with 2.5 mg/ml Proteinase K, 10 mM Tris pH 8.0, 1 mM EDTA and heat, to release viral RNA and inactivate nucleases. DNAzyme cleavage reactions were then performed in 50% heat-treated saliva containing 50 nM DNAzyme and 10 nM RNA transcript in 1× reaction buffer (1× RB containing 50 mM HEPES pH 7.4, 10 mM $MgCl_2$, 100 mM NaCl). The cleavage reaction was first performed at 23 °C for 1 h. Following this step, 50% of the cleavage reaction mixture was taken for the RCA reaction, which was carried out at 23 °C with 10 nM CDT in 1× RCA buffer (50 mM Tris pH 8.0, 10 mM $MgCl_2$, 66 mM KCl, 4 mM DTT, 0.1% Tween 20), in addition to 250 μM dNTP, 1×SYBR Gold, 0.25 U/μl PNK and 0.25 U/μl ϕ29DP.

Three control RCA reactions were also carried out. In Control 1, only CDT was provided, which served as the no-RCA control. Control 2 consisted of CDT and 10 nM DNA primer; the DNA primer has a 20 nt sequence identical to the portion of the RNA cleavage product that binds the CDT and therefore, this control served as the maximal RCA control. Control 3 was performed identically to the test reaction except that the DNAzyme was excluded. This control was used to check the integrity of the RNA substrate (which may get cleaved by nucleases in human saliva and produce background RCA) and to evaluate the dependence of RCA on the presence of the DNAzyme in the cleavage reaction. Additional control reactions containing only DNAzyme in the absence of a control DNA primer were run and showed no direct priming of RCA by DNAzyme sequences (data not shown). Each set of RCA reactions were followed in real time over a period of 2 or 4 h by measuring fluorescence intensity.

Panels A–C of Figure 5 show real-time fluorescence responses for six DNAzyme-RCA coupled systems exemplifying

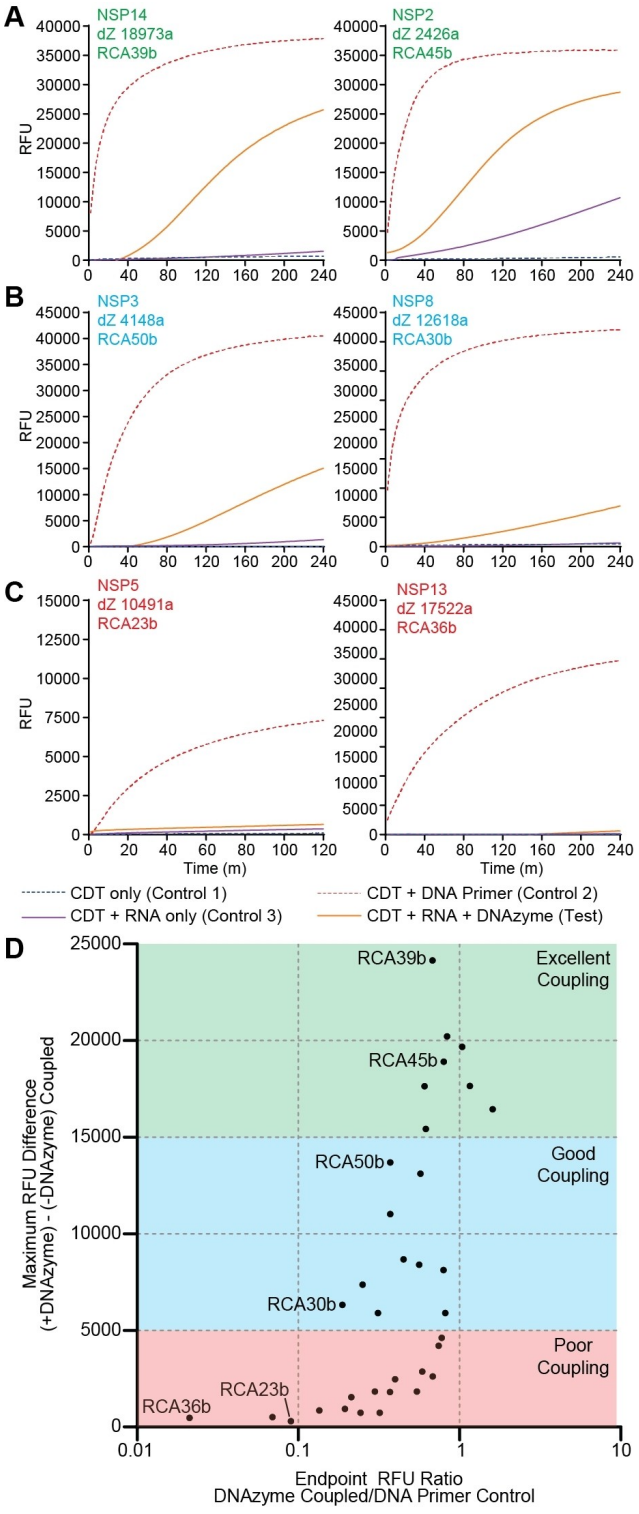

Figure 5. Coupled DNAzyme mediated RNA cleavage and RNA primed RCA reaction. (A–C) RCA fluorescence curves for two excellent, good and poor coupling systems, respectively. Fluorescence data is baselined by subtraction of minimum RFU in negative controls. (D) Summarized RCA coupling screening results. Ratio of DNAzyme coupled RCA vs. RCA Control 2 (RCA with DNA primer) endpoint RFU on X-axis. Maximum RFU difference observed between + DNAzyme and -DNAzyme coupled RCA reactions plotted on Y-axis. All data points are labelled in Figure S23 and RCA CDT sequences are provided in Figure S21.

"Excellent Coupling", "Good Coupling" and "Poor Coupling". The activity of the DNAzyme-coupled RCA reaction (orange curves) is dependent on several factors: 1) the efficiency of RCA for a given CDT; 2) the rate of DNAzyme cleavage of the RNA transcript for generating priming ends; 3) the secondary structure of the RNA cleavage fragment that permits efficient priming of the CDT; and 4) the ability of the CDT to displace the DNAzyme sequence overlapping the RCA priming region after cleavage. Comparing the RCA activity observed from the DNAzyme-containing RNA cleavage reaction (orange curve) to the activity observed with the DNA primer (red dashed curve) gives an overall measure of the efficiency with which the DNAzyme-coupled system can achieve the maximum RCA signal possible from a given CDT. We plotted "Endpoint RFU Ratio" between DNAzyme-coupled RCA and RCA Control 2 as the X-axis of Figure 5D (a fully labelled version of this plot is shown in Figure S23). A second comparison can be made between the RNA cleavage reactions with and without DNAzyme (orange vs. purple curves). An ideal DNAzyme-RCA coupled system would generate a high DNAzyme-dependent signal and a low background signal in the "CDT + RNA only" control (Control 3). Systems with large fluorescence differences between these two reactions are accelerated by the presence of the DNAzyme, presumably due to the generation of more priming RNA molecules by the DNAzyme.

Given the challenge with modelling factors related to sequential reactions of RNA cleavage and RCA as well as the presence of saliva, we plotted the maximum signal (RFU) difference between each pair of RCA reactions with and without DNAzyme as the Y-axis in Figure 5D. This analysis allowed us to generate two important measures of performance for each DNAzyme-RCA coupled system. Points nearest the top-right of the plot correspond to systems that can achieve near-maximum RCA activity in a DNAzyme-dependent manner. The 34 systems are organized into three categories: excellent coupling, good coupling and poor coupling based on the level of DNAzyme-dependent signal enhancement. The "Excellent Coupling" category includes 8 DNAzyme systems that exhibit fluorescence enhancements $>$15,000 RFU in the presence of DNAzyme and all are high on the X-axis, suggesting that systems with excellent coupling require the presence of the DNAzyme. An additional 10 DNAzyme systems, placed in the category of "Good Coupling", which achieve 5,000-15,000 RFU of signal enhancement, also required the presence of the DNAzyme. The remaining 16 DNAzymes are placed in the "Poor Coupling" category as these systems produce low signal enhancement ($<$ 5,000 RFU) with or without coupling with the DNAzyme. Interestingly, such systems span a broad range of dependence on the presence of DNAzymes, suggesting that the presence of the DNAzyme does not guarantee good coupling to RCA.

Comparing DNAzyme cleavage activity in Figure 3 and RCA coupling efficiency in Figure 5D highlights a poor correlation between cleavage activity and coupling efficiency. We hypothesize that the sequence and structure properties required for high-activity DNAzymes are not necessarily the same properties that enable high-efficiency RCA for the reasons discussed above. Hence, screening many efficient DNAzyme/substrate pairs is needed to identify the subset of suitable DNAzyme-RCA coupled systems quickly and effectively for the amplified detection of genomic RNA targets. In this case, screening 34 DNAzyme/substrate pairs produced 8 pairs that show excellent coupling efficiencies, represented by the 8 highest values on the Y-axis, as well as fairly high values on the X-axis.

Achieving amplified detection of RNA transcripts

As a first step toward demonstrating the amplified detection of genomic RNA, we used the dZ 18973a-NSP14-RCA39b system to detect the NSP14 RNA transcript over a range of RNA concentrations, as this system showed excellent DNAzyme coupling and signal enhancement $>$15,000 RFU. We first evaluated the detection of NSP14 RNA using a linear RCA method performed in 1× RB containing 50% human saliva as well as 50 nM DNAzyme and 0.5–50 nM RNA transcript (23 °C for 1 h), followed by RCA in 1× RB containing 50% cleavage reaction mixture and 10 nM CDT for 4 h. However, this method produced a detection limit of only 0.5 nM even after 240 min (Figure S24). To improve the sensitivity of this assay, 100 nM of a second primer P2 was added to bind to the RP (see Table S5 for sequences used in the new assay), which initiated a second stage of amplification, as shown in Figure 6A. This produced a quasi-exponential amplification system (note that an additional primer would be needed to produce a full exponential feedback system). A further optimization of the reporter dye was performed and SYBR Gold was replaced with SYTO 9 nucleic acid stain to reduce inhibition of the RCA reaction observed with SYBR Gold (data not shown).[36]

Using conditions identical to those employed for linear RCA, except for the inclusion of 100 nM of P2 and 2 μM SYTO 9 instead of 1× SYBR Gold, a substantially improved fluorescence response was obtained (see Figure 6B), providing a detection limit of 500 aM (~200 copies/μL) of RNA after 6 h (Figure 6C), although a significant fluorescence increase was also observed in the control reaction due to the high concentration of P2. This represents an improvement of over 6 orders of magnitude relative to linear RCA (Figure 6C) and provides a dynamic range that covers at least 8 orders of magnitude of RNA concentration, and more importantly, demonstrates that coupling RNA cleavage by the 10-23 DNAzyme to RCA can be used to detect long RNA transcripts at clinically relevant concentrations.

Validating the method with patient samples

To evaluate the clinical utility of the new assay and confirm that it was capable of detecting the full genomic RNA of SARS-CoV-2 in a real-world sample, we examined a panel of 29 patient saliva samples, including 14 positive and 15 negative samples. Table S6 provides details on each sample, including NPS and saliva-based C_t values obtained from RT-PCR along with the presumed variant (for positive samples). The dZ 18973a-NSP14-RCA39b system evaluated with RNA transcripts was also used for testing of patient samples. The samples were treated using

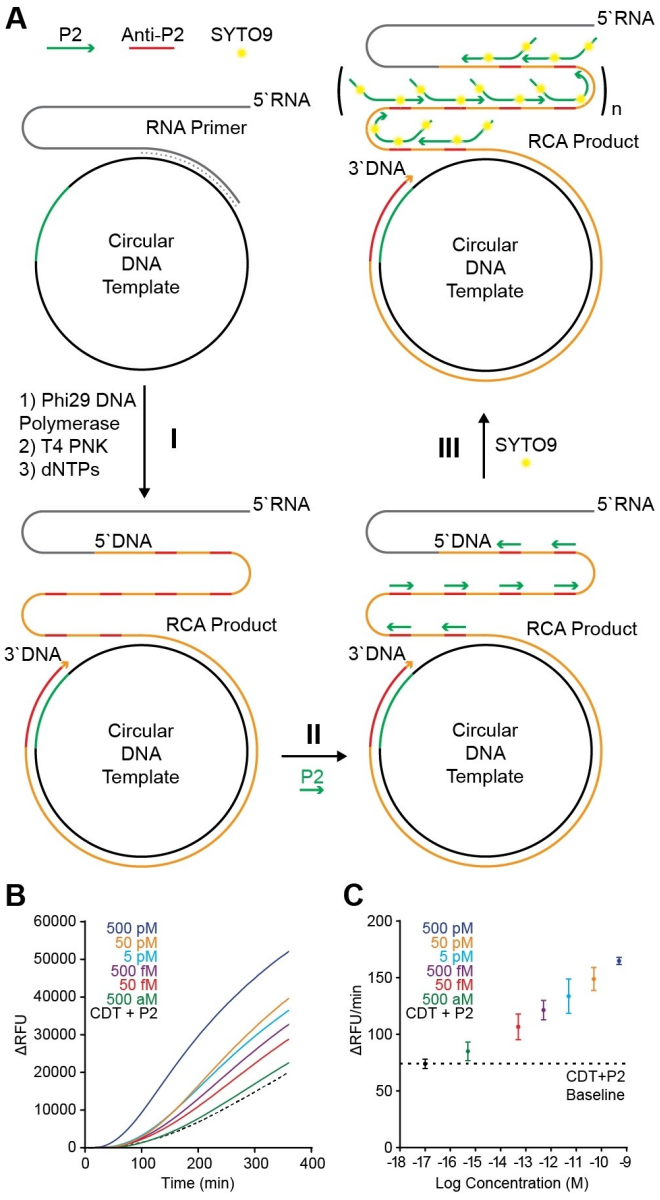

Figure 6. (A) Quasi-exponential RCA reaction scheme. P2 is designed to bind to RCA product, initiating a second stage of amplification. (B) Normalized fluorescence vs. time for the listed RCA reactions. (C) Normalized rate of reaction vs. log [RNA]. Rate of reaction calculated by taking the slope of linear portion of each curve in panel B.

the optimized saliva processing method described above to digest contaminating proteins and release viral RNA (12 min), followed by incubating the saliva samples with DNAzyme and reaction buffer for the RNA cleavage reaction (60 min) and then performing the RCA reaction with real-time monitoring using a Bio-Rad CFX-96 real-time thermal cycler (60 min) (Figure 7A). The total sample to readout time was under 2.5 h.

Data were analyzed using both endpoint RFU at 60 min RCA reaction time, and the increase in RFU over time. Both methods provided excellent discrimination between positive and negative samples, however we chose to use endpoint RFU values owing to simplicity of data collection. Figure 7B shows box plots for endpoint RFU max/min, interquartile ranges and medians for positive and negative samples, and clearly indicates distinct differences in endpoint RFU between saliva samples collected from patients diagnosed with SARS-CoV-2 (positive) and those without the infection. Figure 7C shows the RFU measured for each of the individual saliva samples (PS# and NS#), along with high (positive: PC) and low (negative: NC) controls (see Figure S25 for a full set of control data). Based on a Receiver Operating Characteristic (ROC) curve (Figure 7D), we determined the clinical cut-off value to be 22,000 RFU, which resulted in a sensitivity of 86% (true positives detected), a specificity of 100% (true negatives detected), and an overall accuracy of 93%.

An Important point to note In Figure 7C Is that all of the negative saliva samples showed amplification values greater than that of the negative control. It is possible that endogenous human RNA may either be cleaved by the DNAzyme or may directly prime the CDT, leading to the relatively high background.

It is also conceivable that the dye can bind to background RNA in the saliva samples as extraction and digestion steps were not performed; salivary DNA as well as P2 and the CDT can also contribute to background signals. To evaluate these possibilities, control experiments were performed on a subset of positive and negative samples where either the DNAzyme or CDT were excluded (Figure S25). In each case, the endpoint RFU was highest with both species present, lower when the DNAzyme was excluded, and lowest when the CDT was absent. This confirms that the CDT is capable of amplifying either viral or endogenous RNA even when the DNAzyme is absent, though addition of DNAzyme produces additional amplification. This data also shows that the DNAzyme significantly improves the discrimination between positive and negative samples. We believe this enhancement is due to the ability of the DNAzymes to generate 3′ RNA terminals in close proximity to the CDT, thereby accelerating the initiation of RCA. However, these controls show that further optimization of sample processing steps and CDT sequence will be needed to aid in lowering background signals.

An important point from Figure 7C is that the detection of SARS-CoV-2 in positive patients does not depend on the variant. Given that the target site of the dZ 18973a-NSP14-RCA39b system is not known to be mutated between the different SARS-CoV-2 variants, a variant dependent effect would not be expected when using this target site. The high targeting specificity of DNAzymes does offer the potential for further development of this method to enable variant discrimination. A multiplex assay design can be envisaged where multiple DNAzyme-RCA systems, each sensitive to a specific mutation, are combined and the resulting signal patterns are signatures for specific variants.

Comparing with other molecular tests

Table S7 compares this newly developed assay to several recently reported saliva-based SARS-CoV-2 molecular tests. Both

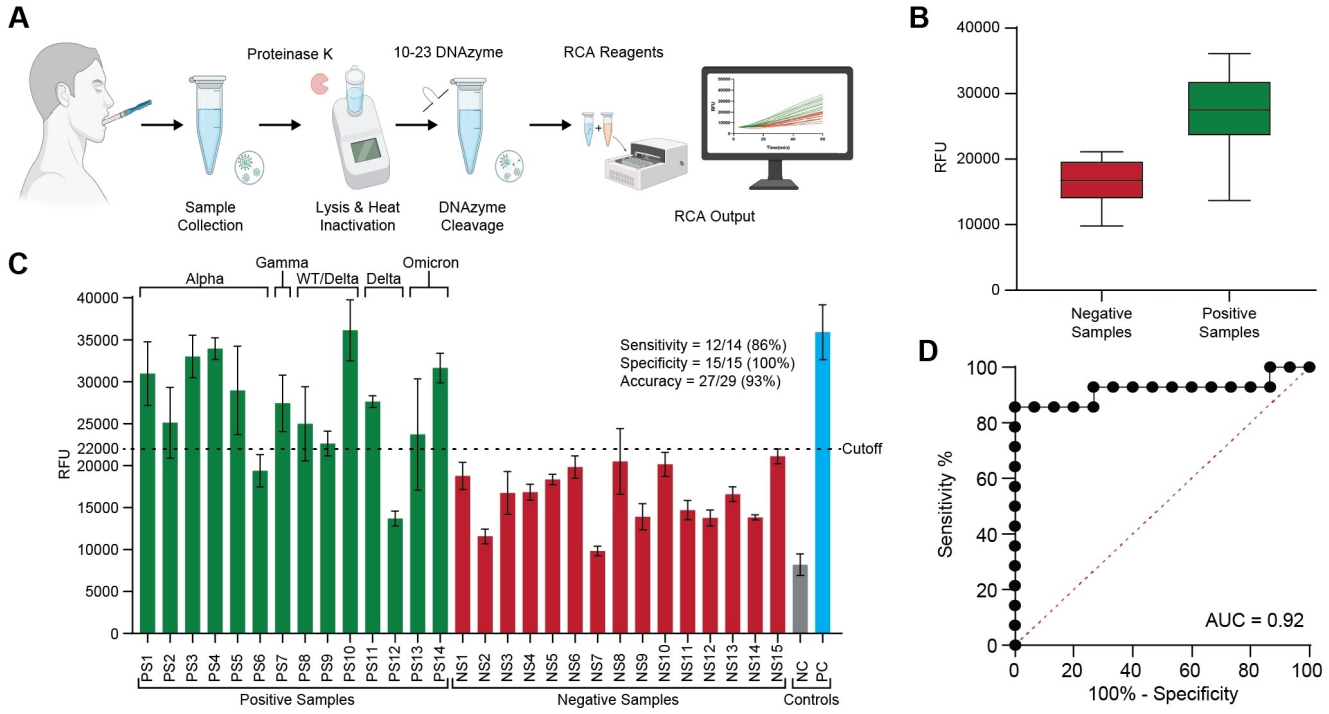

Figure 7. (A) Schematic of the assay. Sample collection is followed by Proteinase K and heat treatment, DNAzyme cleavage reaction incubated at room temperature for 1 h and subsequent RCA and signal readout. RFU signal measured over time using Bio-Rad CFX-96 real-time thermal cycler for 1 h (B) Box plot showing distribution (minimum, maximum, interquartile range and median) of the endpoint RFU values for 14 positive (green) patient saliva samples (Alpha, Gamma, WT, Delta and Omicron variants) and 15 negative (red) patient saliva samples. SARS-CoV-2 variant indicated above bars. WT/Delta classification indicates an indeterminant variant based on variant PCR and prevalence. (C). Bar plot representing the mean endpoint RFU for a given sample Dotted line indicates the cut-off point for the assay. The error bars represent the one standard deviation from the mean obtained from triplicate measurements. (D) Receiver Operating Characteristic (ROC) plot of coupled DNAzyme-RCA assay using mean RFU data and cut-off value from Panel C.

the limit of detection (viral copies per microliter) and test time for this method are slightly poorer than previously reported saliva-based SARS-CoV-2 molecular tests, though both of these parameters could likely be improved by moving to a fully exponential RCA assay. Even so, key metrics including clinical sensitivity (86%) and specificity (100%) are comparable to and, in some cases, better than previous saliva-based SARS-CoV-2 molecular tests. Our new test is also capable of detecting multiple SARS-CoV-2 variants, though this was not generally reported for previous tests. Hence, the DNAzyme-coupled RCA assay represents a promising method for rapid and reliable SARS-CoV-2 RNA detection in saliva.

Conclusions

In summary, we report on a new method for amplified detection of genomic RNA based on DNAzyme-mediated RNA cleavage coupled to RCA. For large and highly structured RNA sequences such as the genomic RNA of SARS-CoV-2, we show that it is possible to screen a large set of DNAzymes using RNA transcripts to quickly identify those that have the highest cleavage activity. This is the first report to use such a screening approach, and represents a quick, simple and cost-effective approach for finding DNAzymes that target suitable RNA sites for binding and cleavage. This method overcomes the issue of inaccessibility of RNA sequences due to the formation of secondary and tertiary structures. We also demonstrate the ability to further screen effective DNAzyme/substrate pairs in the cleavage reaction for coupling to RCA, which represents an efficient way to find excellent systems for RCA. Importantly, this study also shows that the DNAzyme-mediated RCA approach can be implemented for amplified detection of RNA in human saliva, and for detection of SARS-CoV-2 genomic RNA in positive patient saliva samples.

Experimental Section

RNA cleavage site selection: DNAzymes were designed using the 10-23 catalytic core.[34] RNA secondary structure prediction for various SARS-CoV-2 genes was determined using RNAfold (http://rna.tbi.univie.ac.at/) configured to use the Andronescu 2007 RNA energy parameters.[37,38] DNAzyme targets were manually selected based on the location of cleavable dinucleotide junctions (A–U and G–U), located in unstructured regions (single-stranded regions) or low probability structures.

DNAzyme screening reactions: DNAzyme cleavage reactions were performed using 500 nM DNAzyme and 6000 cpm (< 50 nM) radiolabeled RNA transcript. Reaction mixtures were heated at 90 °C for 1 min and cooled to room temperature for 5 min to anneal. Cleavage was initiated by addition of reaction buffer to 1×(1×: RB; 50 mM HEPES pH 7.4, 10 mM $MgCl_2$, 100 mM NaCl). Reactions were incubated at 23 °C for 10 min and stopped by addition of

quenching buffer (QB) to 1×(10% sucrose, 1×TBE, 4 M urea, 30 mM EDTA, 0.14 mg/ml xylene cyanol and bromophenol blue). Cleavage reactions were resolved on 5% or 10% dPAGE, exposed on a storage phosphor screen and imaged using a Typhoon FLA 9500 Biomolecular Imager (Cytiva) at the Centre for Microbial and Chemical Biology (McMaster University). Gel images were analysed using Image J (https://imagej.nih.gov).[39]

Quasi-exponential RCA system: A quasi-exponential RCA system was developed to improve the sensitivity of the DNAzyme-coupled RCA method. The DNAzyme-cleaved RNA (P1) primes the circle to generate reaction products (RPs), followed by a second primer (P2) binding to each tandem repeat of the RP. As the original RCA strand elongates, new priming sites for P2 are generated. The result of the two priming events is an accelerated increase in RPs over time and hence an improvement in sensitivity compared to linear RCA. The lack of a feedback process and P1 being a limiting factor prevents the system from performing full exponential amplification.

Quasi-exponential RCA was employed to determine the limit of detection of this assay. As described in the previous section, cleavage reactions containing 50% (v/v) heat-inactivated saliva, 50 nM DNAzyme and a range of RNA transcript concentrations from 0.5 nM0.5 fM were initiated by addition of RB to 1× and incubated at 23 °C for 1 h. Following DNAzyme cleavage, half the reaction was taken for RCA and set up as follows: 50% (v/v) DNAzyme reaction mixture, 10 nM CDT, 100 nM P2, 250 μM of each dNTP, 2 μM SYTO 9, 0.25 U/μl PNK, 0.25 U/μl phi29 DNA Polymerase, phi29 reaction buffer (PB). One RCA control reaction containing 10 nM CDT and 100 nM P2 (no RNA and saliva) was set up. Final reaction volumes were 20 μL. All reactions conducted in triplicate and were incubated at 23 °C in a Bio-Rad CFX-96 real-time thermal cycler for 6 h while monitoring fluorescence using the FAM/SYBR filter.

Baseline subtracted fluorescence for listed RCA reactions plotted as ΔRFU vs. time is shown in Figure 6B. The RFU value at the first reading point (T = 0) was subtracted from the value at each final time point to determine ΔRFU. The rate of reaction (change in RFU with time) vs. log [RNA] is shown in Figure 6C. The rate was calculated by taking the slope of the linear portion of each curve (from T = 100 min to T = 360 min), with error bars representing one standard deviation from the mean obtained from triplicate measurements. All graphs were generated using GraphPad Prism.

Clinical evaluation of patient saliva samples: Collection of saliva specimens was performed using a protocol approved by the Hamilton Integrated Research Ethics Board (HiREB Project # 12636). Patients attending COVID-19 assessment centers at sites operated by Hamilton Health Sciences or St. Joseph's Healthcare in Hamilton, Ontario, were invited to donate a supervised, self-collected, drool saliva sample immediately following collection of a nasopharyngeal swab (NPS). Saliva specimens were stored at 4 °C during transport (< 72 h) and subsequently long-term at −80 °C. NPS specimens collected for standard COVID-19 screening were tested using a standard RT-PCR method by the Hamilton Regional Laboratory Medicine Program at St. Joseph's Healthcare, Hamilton. NPS test results were used to identity candidate negative (15 patients, NS1-15) and positive saliva specimens (14 patients, PS1-14), and to assign putative variants to each positive sample. The presence of SARS-CoV-2 in candidate saliva specimens was further confirmed using a saliva RT-PCR method described previously.[40,41]

All saliva samples were processed as described in the "Coupled DNAzyme-RCA Reactions" section, and samples were tested using the quasi-exponential RCA protocol as described in "Quasi-exponential RCA System". Control reactions, set up and performed in parallel without saliva included a positive control with CDT, 50 nM DNAzyme, 10 nM RNA transcript and a negative control with CDT and P2 only. The assay was run for 3 h; all RFU curves were baselined to the minimum observed RFU across all samples at T = 0 and values at 60 min were used to prepare box plots (Figure 7B) and column plots (Figure 7C). Data at 60 min as the endpoint RFU value as background fluorescence for the negative control reaction started rising past this timepoint. Data was plotted using a Receiver Operating Characteristic plot, and the cut-off was the value that maximized the sum of sensitivity and specificity to determine the number of true positives and true negatives identified by the assay. Additional control reactions presented in Figure S25 were prepared by selecting 3 positive and 3 negative patient samples. Reactions were performed as described previously with the following modifications: 1) exclusion of DNAzyme, or 2) exclusion of DNAzyme and CDT (Figure S25).

Author Contributions

YL, JDB, JG, CDMF, LS, KM and AC designed the experiments and interpreted the data. GP, BJS, CB, JG and DY oversaw collection of patient saliva samples. DW performed PCR analysis on patient saliva samples. JG, CN and AM performed all DNAzyme and RCA experiments and analyzed the data. YL, JDB, CF, AM, CN and JG wrote the manuscript. All authors edited the manuscript.

Acknowledgements

Funding for this work was provided by the Canadian Institutes for Health Research (CIHR; Grant No. 446898), the Canadian Foundation for Innovation (CFI; Grant No. 20339), the Ontario Ministry for Research and Innovation (ORF-RE; Grant No. RE07-045). We thank Prof. Gerry Wright, Haley Zubyk and Jianrun Xia for providing and preparing vectors used to generate RNA transcripts. LS holds the Canada Research Chair (CRC) in Miniaturized Biomedical Devices and an Ontario Early Researcher Award. JDB holds the CRC in Point-of-Care Diagnostics.

Conflict of Interest

The authors declare no conflict of interest.

Data Availability Statement

The data that support the findings of this study are available in the supplementary material of this article.

Keywords: biosensors · COVID-19 · DNAzyme · RNA recognition · rolling circle amplification

[1] A. Esquela-Kerscher, F. J. Slack, *Nat. Rev. Cancer* **2006**, *6*, 259–269.
[2] M. S. Nicoloso, R. Spizzo, M. Shimizu, S. Rossi, G. A. Calin, *Nat. Rev. Cancer* **2009**, *9*, 293–302.
[3] O. Wapinski, H. Y. Chang, *Trends Cell Biol.* **2011**, *21*, 354–361.

[4] S. Paik, S. Shak, G. Tang, C. Kim, J. Baker, M. Cronin, F. L. Baehner, M. G. Walker, D. Watson, T. Park, W. Hiller, E. R. Fisher, D. L. Wickerham, J. Bryant, N. Wolmark, *N. Engl. J. Med.* **2004**, *351*, 2817–2826.
[5] E. Senkus, S. Kyriakides, F. Penault-Llorca, P. Poortmans, A. Thompson, S. Zackrisson, F. Cardoso, ESMO Guidelines Working Group, *Ann. Oncol.* **2013**, *24 Suppl 6*, vi7–23.
[6] E. N. Imyanitov, A. G. Iyevleva, E. V. Levchenko, *Crit. Rev. Oncol. Hematol.* **2021**, *157*, 103194.
[7] A. J. Baeumner, R. N. Cohen, V. Miksic, J. Min, *Biosens. Bioelectron.* **2003**, *18*, 405–413.
[8] B. Tian, F. Gao, J. Fock, M. Dufva, M. F. Hansen, *Biosens. Bioelectron.* **2020**, *165*, 112356.
[9] E. Xiong, L. Jiang, T. Tian, M. Hu, H. Yue, M. Huang, W. Lin, Y. Jiang, D. Zhu, X. Zhou, *Angew. Chem. Int. Ed.* **2021**, *60*, 5307–5315; *Angew. Chem.* **2021**, *133*, 5367–5375.
[10] P. Moitra, M. Alafeef, K. Dighe, M. B. Frieman, D. Pan, *ACS Nano* **2020**, *14*, 7617–7627.
[11] Y. Peng, Y. Pan, Z. Sun, J. Li, Y. Yi, J. Yang, G. Li, *Biosens. Bioelectron.* **2021**, *186*, 113309.
[12] G. A. Santiago, E. Vergne, Y. Quiles, J. Cosme, J. Vazquez, J. F. Medina, F. Medina, C. Colón, H. Margolis, J. L. Muñoz-Jordán, *PLoS Neglected Trop. Dis.* **2013**, *7*, e2311.
[13] S. A. Byron, K. R. Van Keuren-Jensen, D. M. Engelthaler, J. D. Carpten, D. W. Craig, *Nat. Rev. Genet.* **2016**, *17*, 257–271.
[14] S. C. Taylor, K. Nadeau, M. Abbasi, C. Lachance, M. Nguyen, J. Fenrich, *Trends Biotechnol.* **2019**, *37*, 761–774.
[15] L. M. Styer, T. T. Miller, M. M. Parker, *J. Clin. Virol. Off. Publ. Pan Am. Soc. Clin. Virol.* **2013**, *58 Suppl 1*, e127–133.
[16] Y.-Z. Zheng, J.-T. Chen, J. Li, X.-J. Wu, J.-Z. Wen, X.-Z. Liu, L.-Y. Lin, X.-Y. Liang, H.-Y. Huang, G.-C. Zha, P.-K. Yang, L.-J. Li, T.-Y. Zhong, L. Liu, W.-J. Cheng, X.-N. Song, M. Lin, *Front. Cell. Infect. Microbiol.* **2021**, *11*, 613304.
[17] L. Yan, J. Zhou, Y. Zheng, A. S. Gamson, B. T. Roembke, S. Nakayama, H. O. Sintim, *Mol. BioSyst.* **2014**, *10*, 970–1003.
[18] J. R. Mora, R. C. Getts, *Expert Rev. Mol. Diagn.* **2007**, *7*, 775–785.
[19] L. Xu, J. Duan, J. Chen, S. Ding, W. Cheng, *Anal. Chim. Acta* **2021**, *1148*, 238187.
[20] N.-I. Goo, D.-E. Kim, *Biochip J.* **2016**, *10*, 262–271.
[21] M. M. Ali, F. Li, Z. Zhang, K. Zhang, D.-K. Kang, J. A. Ankrum, X. C. Le, W. Zhao, *Chem. Soc. Rev.* **2014**, *43*, 3324–3341.
[22] R. M. Bialy, A. Mainguy, Y. Li, J. D. Brennan, *Chem. Soc. Rev.* **2022**, *51*, 9009–9067.
[23] D. P. Kalogianni, P. M. Kalligosfyri, I. K. Kyriakou, T. K. Christopoulos, *Anal. Bioanal. Chem.* **2018**, *410*, 695–713.
[24] H. Dong, J. Lei, L. Ding, Y. Wen, H. Ju, X. Zhang, *Chem. Rev.* **2013**, *113*, 6207–6233.
[25] J. Ye, M. Xu, X. Tian, S. Cai, S. Zeng, *J. Pharm. Anal.* **2019**, *9*, 217–226.
[26] D. Kim, J.-Y. Lee, J.-S. Yang, J. W. Kim, V. N. Kim, H. Chang, *Cell* **2020**, *181*, 914–921.e10.
[27] S. W. Santoro, G. F. Joyce, *Proc. Nat. Acad. Sci.* **1997**, *94*, 4262–4266.
[28] M. J. Cairns, *Nucleic Acids Res.* **2003**, *31*, 2883–2889.
[29] A. Serganov, D. J. Patel, *Nat. Rev. Genet.* **2007**, *8*, 776–790.
[30] P. Michalak, M. Soszynska-Jozwiak, E. Biala, W. N. Moss, J. Kesy, B. Szutkowska, E. Lenartowicz, R. Kierzek, E. Kierzek, *Sci. Rep.* **2019**, *9*, 3801.
[31] R. P. Smyth, M. Negroni, A. M. Lever, J. Mak, J. C. Kenyon, *Front. Immunol.* **2018**, *9*, 2097.
[32] F. Wu, S. Zhao, B. Yu, Y.-M. Chen, W. Wang, Z.-G. Song, Y. Hu, Z.-W. Tao, J.-H. Tian, Y.-Y. Pei, M.-L. Yuan, Y.-L. Zhang, F.-H. Dai, Y. Liu, Q.-M. Wang, J.-J. Zheng, L. Xu, E. C. Holmes, Y.-Z. Zhang, *Nature* **2020**, *579*, 265–269.
[33] R. de C. A. Tavares, G. Mahadeshwar, H. Wan, N. C. Huston, A. M. Pyle, *J. Virol.* **2021**, *95*, e02190–20.
[34] S. W. Santoro, G. F. Joyce, *Biochemistry* **1998**, *37*, 13330–13342.
[35] A. R. Gruber, R. Lorenz, S. H. Bernhart, R. Neuböck, I. L. Hofacker, *Nucleic Acids Res.* **2008**, *36*, W70-W74.
[36] T. L. Quyen, T. A. Ngo, D. D. Bang, M. Madsen, A. Wolff, *Front. Microbiol.* **2019**, *10*.
[37] R. Lorenz, S. H. Bernhart, C. Höner Zu Siederdissen, H. Tafer, C. Flamm, P. F. Stadler, I. L. Hofacker, *Algorithms Mol. Biol. AMB* **2011**, *6*, 26.
[38] M. Andronescu, A. Condon, H. H. Hoos, D. H. Mathews, K. P. Murphy, *Bioinforma. Oxf. Engl.* **2007**, *23*, i19–28.
[39] C. A. Schneider, W. S. Rasband, K. W. Eliceiri, *Nat. Methods* **2012**, *9*, 671–675.
[40] D. R. E. Ranoa, R. L. Holland, F. G. Alnaji, K. J. Green, L. Wang, C. B. Brooke, M. D. Burke, T. M. Fan, P. J. Hergenrother, *bioRxiv* **2020**, 2020.06.18.159434.
[41] D. White, J. Gu, C.-J. Steinberg, D. Yamamura, B. J. Salena, C. Balion, C. D. M. Filipe, A. Capretta, Y. Li, J. D. Brennan, *Sci. Rep.* **2022**, *12*, 2806.

Manuscript received: January 9, 2023
Accepted manuscript online: February 15, 2023
Version of record online: March 27, 2023